Developmental Biology 445 (2019) 16–28

Contents lists available at ScienceDirect

Developmental Biology

journal homepage: www.elsevier.com/locate/developmentalbiology

A cell surface protein controls endocrine ring gland morphogenesis and steroid production

Yanina-Yasmin Pesch[a,b,c], Ricarda Hesse[a], Tariq Ali[a], Matthias Behr[a,b,*]

[a] Institute for Biology and Saxon Incubator for Clinical Translation (SIKT), University of Leipzig, Philipp-Rosenthal-Str. 55, 04103 Leipzig, Germany
[b] Life & Medical Sciences Institute (LIMES), University of Bonn, 53115 Bonn, Germany
[c] Department of Cellular and Physiological Sciences, University of British Columbia, Vancouver, Canada BC V6T 1Z3

ARTICLE INFO

Keywords:
Axon
Cuticle
Ecdysone
Endocytosis
Extracellular matrix
Fasciclin2
Obstructor-A
Ring gland
Steroid
Trachea

ABSTRACT

Identification of signals for systemic adaption of hormonal regulation would help to understand the crosstalk between cells and environmental cues contributing to growth, metabolic homeostasis and development. Physiological states are controlled by precise pulsatile hormonal release, including endocrine steroids in human and ecdysteroids in insects. We show in *Drosophila* that regulation of genes that control biosynthesis and signaling of the steroid hormone ecdysone, a central regulator of developmental progress, depends on the extracellular matrix protein Obstructor-A (Obst-A). Ecdysone is produced by the prothoracic gland (PG), where sensory neurons projecting axons from the brain integrate stimuli for endocrine control. By defining the extracellular surface, Obst-A promotes morphogenesis and axonal growth in the PG. This process requires Obst-A-matrix reorganization by Clathrin/Wurst-mediated endocytosis. Our data identifies the extracellular matrix as essential for endocrine ring gland function, which coordinates physiology, axon morphogenesis, and developmental programs. As Obst-A and Wurst homologs are found among all arthropods, we propose that this mechanism is evolutionary conserved.

1. Introduction

Steroid hormones are small, lipophilic compounds that can pass through cell membranes and constitute important regulators of growth, metabolism, and reproduction (Sapolsky et al., 2000). To coordinate steroid production neuronal and endocrine systems need to integrate external and internal cues in the vertebrate hypothalamic-pituitary system. Furthermore, reciprocal interactions between nerves and glands maintain homeostasis and allow for responses to environmental stimuli. As a response to stimulatory and inhibitory signals coming from the hypothalamus, pituitary gland cells synthesize and secrete a variety of specific pituitary trophic hormones, such as ACTH (adrenocorticotropic hormone), Thyroid stimulating hormone (TSH), and Follicle stimulating hormone (FSH), in a pulsatile and episodic manner. Any malfunctions in the interactions between nerves and the pituitary gland can lead to multiple endocrine disorders, neurological manifestations and has substantial impact on metabolism, sexual maturation, reproduction, blood pressure and other vital physical functions (Bancalari et al., 2012; Melmed, 2003; Muglia et al., 2000; Yeung et al., 2006; Yu, 2014).

In *Drosophila* distinct neurosecretory cells from the brain stimulate hormone responses in the endocrine ring gland (Yamanaka et al., 2013). Most prominent Prothoracicotropic hormone (PTTH) expressing neurosecretory cells project axons from the brain to directly stimulate ecdysone steroid production (McBrayer et al., 2007; Shimada-Niwa and Niwa, 2014). In addition, other neuroendocrine centers in the brain send axons through the nervus corporis cardiaci (Ncc) NccI and NccIItowards the ring gland (Siegmund and Korge, 2001; Velasco et al., 2007). The ring gland itself is formed by the two prothoracic gland (PG, ventrally) lobes, corpora allata (CA, dorsally), and corpora cardiaca (CC, laterally) (Sanchez-Higueras et al., 2014). The CC cells affect metabolism by secreting Adipokinetic Hormone (AKH) for manipulating sugar levels in the hemolymph, as well as glycemic factors and heart rate accelerating peptides/hormones (Kim and Rulifson, 2004; Siegmund and Korge, 2001; Velasco et al., 2004). *Drosophila* that lack the CA, which is the source of JH, pupariated at smaller size due to reduced larval growth rates and were lethal at pupal stages (Jindra et al., 2013; Riddiford et al., 2010). Most of the ring gland volume is taken up by the PGs, whose cells grow in size, while CC cells remain small (Velasco et al., 2004). PG cells produce and secrete the steroid hormone ecdysone. Thus, insect development and metamorphosis is coordinately controlled by the sesquiterpenoid juvenile

* Corresponding author at: Institute for Developmental Biology and Saxon Incubator for Clinical Translation (SIKT), University of Leipzig, Philipp-Rosenthal-Str. 55, 04103 Leipzig, Germany.
E-mail address: matthias.behr@uni-leipzig.de (M. Behr).

https://doi.org/10.1016/j.ydbio.2018.10.007
Received 10 August 2018; Received in revised form 9 October 2018; Accepted 15 October 2018
Available online 24 October 2018
0012-1606/

hormones (JH) and the molting hormone 20-hydroxyecdysone (20E).

Ecdysone biosynthesis relies on dietary cholesterol which is processed by a number of enzymes. Npc1a protein, named after the Niemann-Pick type C disease, is required for providing cholesterol as substrate for ecdysone biosynthesis (Danielsen et al., 2016; Huang et al., 2005). In the PGs sterols are then converted into Ecdysone by subsequent modifications regulated by a number of ecdysteroidogenic enzymes encoded by *neverland* and the *Halloween* genes such as *spook, shroud* and *phantom* (Di Cara and King-Jones, 2013; Niwa and Niwa, 2014; Rewitz et al., 2013). Secreted from PGs, Ecdysone is released into the circulatory system and converted into the more active 20 hydroxyecdysone (20E) by the P450 (Halloween) enzyme Shade. 20E finally binds and controls the activity of the nuclear ecdysone receptor complex to initiate transcription of many target genes that precisely regulate larval molting and metamorphosis (King-Jones and Thummel, 2005; Niwa and Niwa, 2014; Yamanaka et al., 2015, 2013). The activated EcR/Usp receptor complex binds genomic response elements to initiate transcription of early response target genes, of which *E74A* is a prominent representative (Johnston et al., 2011; Parvy et al., 2005; Yamada et al., 2000). The Cyp18a1 enzyme is involved in the termination of ecdysone pulses by feedback mechanism (Rewitz et al., 2010). Finally, ecdysis-triggering hormones (ETH) trigger centrally patterned ecdysis and accompanied behaviors by induction of the eclosion hormone (EH) and its release from neurosecretory cells (Kingan et al., 1997; Kruger et al., 2015; Park et al., 2002).

Obstructor (Obst)-A belongs to the *Drosophila obstructor* multigene family which is well-conserved among arthropods (Behr and Hoch, 2005; Jasrapuria et al., 2010). The Obst-A protein is characterized by three Chitin-binding domains type 2 (CBDs), a specific domain composition that has been identified even in nematodes (Behr and Hoch, 2005). Obst-A is expressed in ectodermal epithelia and secreted towards the extracellular space where it is located at the chitinous matrix. Acting as a scaffold-like protein Obst-A binds chitin and recruits other proteins and enzymes for chitin-matrix growth. Obst-A modulates localization of proteins and enzymes at the extracellular matrix that in turn control physical and chemical properties. Thereby Obst-A affects cuticle stiffness during wound repair and integrity against numerous stresses (Pesch et al., 2016, 2015; Petkau et al., 2012). Here we report surprising evidence that Obst-A is needed for proper ring gland morphogenesis. Immunofluorescent studies show that Obst-A defines the extracellular matrix (ECM) of PG cells. Mutant studies further confirm that the extracellular Obst-A-matrix is required for upregulation of RNA levels of ecdysteroidogenic enzyme genes for the PG in the onset of ecdysis. Genetic studies indicate further that normal axon growth at the PG surface depends on the Obst-A defined PG matrix. We show that axons in *obst-A* null mutants and PG specific knockdown embryos are prevented from normal growth at the PG. This would be consistent with the fact that not only chemical signals but also substrate properties, such as stiffness can determine axon growth (Koser et al., 2016). Finally, extracellular Obst-A localization and its functional consequences for PG cells depends on its internalization via Wurst/Clathrin-mediated endocytosis. Since both Obst-A and Wurst (orthologous to vertebrate DNAJC22) proteins are largely conserved, their roles in steroid control is potentially relevant to all arthropods.

2. Materials and methods

2.1. Fly husbandry

Flies were derived from the following sources: w^{1118} (referred to as wt); P0206-Gal4 and Aug21-Gal4 (Mirth et al., 2005); ptth-Gal4 (McBrayer et al., 2007); *obst-A*^{d03} (Petkau et al., 2012), hemizygous *obst-A* mutant larvae were selected for the absence of actin-GFP expression, FM7 actin-GFP positive heterozygous animals were used as control; UAS-*obst-A* (Petkau et al., 2012); gartenzwerg (garz)^{EMS667} (Wang et al., 2012) other Gal4 lines (69B-Gal4, Mai60-Gal4, akh-Gal4), UAS-shi$^{DN\ (K44A)}$ and UAS *obst-A*-RNAi (VDRC ID 102591, KK library, no off targets) line were obtained from Vienna and Bloomington stock centers. For knockdown analysis, Gal4 flies were mated with UAS flies and progeny was incubated at 29 °C. As RNAi induced phenotypes can be variable to some extent, we show representative images of observed phenotypes and indicate the number of analyzed animals. For analyzing development of RNAi knockdown, control and *obst-A* rescue animals we collected and freshly hatched larva were transferred onto fresh agar plates (10–25 animals per plate) with instant yeast. Larvae were monitored repeatedly every 24 h. Developmental status was documented accordingly (Vaufrey et al., 2018). The shape phenotypes of *obst-A* rescue males were documented with a Zeiss Stemi 508, a Axiocam 105 color, and ZEN.

2.2. Preparations of animals and immunofluorescent analysis

Embryos were prepared, fixed with 4% formaldehyde, intensively washed in PBT (PBS, Tween20). Primary antibodies were incubated overnight at 4 °C (exceptions: Wurst 72 h at 4 °C), washed with PBT and incubated with secondary antibodies overnight at 4 °C. After washing embryos were mounted in Vectashield (Vector Laboratories). Larvae were dissected and fixed for 1 h in 4% formaldehyde as described recently (Pesch et al., 2017). For immunofluorescent staining, the following primary antibodies were used as described previously (Pesch et al., 2015; Petkau et al., 2012; Stümpges and Behr, 2011), summarized below:

Antibody	Dilution	Host animal	Origin
anti-Chc	1:80	Rat	(Wingen et al., 2009)
anti-Fas2 (1D4)	1:75	Mouse	DSHB
anti-Fas3 (7G10)	1:50	Mouse	DSHB
anti-EcR (10F1)	1:10	Mouse	DSHB
anti-Phospho-Histone, Ser10	1:100	Rabbit; #9701	Cell signaling
anti-Knk	1:100	Rabbit	(Moussian et al., 2006)
anti-Obst-A	1:75	Rabbit	(Petkau et al., 2012)
anti-Serp	1:100	Rabbit	(Luschnig et al., 2006)
anti-Spalt	1:50	Rabbit	(Kuhnlein et al., 1994)
anti-α-Spectrin (3A9)	1:10	Mouse	DSHB
anti-Verm	1:100	Rabbit	(Luschnig et al., 2006)
anti-Wurst	1:50	Guinea pig	(Stümpges and Behr, 2011; Wingen et al., 2009)

Chitin was detected with CBP, Chitin-binding-probe, tagged with Alexa488 (Pesch et al., 2015); Alexa633-conjugated Wheat Germ Agglutinin (WGA; 1:250; Molecular Probes, Carlsbad, USA) is a lectin that detects N-acetylglucosamine and N-acetylneuraminic acid residues, thereby labeling cell surfaces of many embryonic and larval tissues (Pesch et al., 2017). Secondary antibodies conjugated with fluorescent dyes (Dianova, Hamburg, Germany and JacksonImmuno, Baltimore, USA) were used.

Larval tissues were dissected and mounted in Fluoromount-G with DAPI (SouthernBiotech, Birmingham, USA). Embryos were mounted in Vectashield with DAPI. Stainings were analyzed with at least in general $n \geq 5$ imaged ring glands/animals per genetic condition. Confocal stainings were imaged with a Zeiss LSM780 (Carl Zeiss, Jena, Germany). The confocal Spinning Disc image was taken by sequential scans with a Zeiss Cell Observer, the Yokogawa spinning disc scanning unit and dual Axiocams 503 m. Images were taken with 63x LCI Plan Neofluar and 63x Plan-Apochromatic Objectives. The

laser (405 nm, 488 nm, 560 nm, 633 nm) and filter settings were adjusted to avoid cross-talk. Zeiss Airyscan standard setting were used and Z-stacks were performed with optimal distances calculated by the Zen software. Airyscan raw data were further processed by the Zeiss ZEN AiryScan software. For deconvolution of standard confocal images Autoquant X3 software (Bitplane, USA) and ZEN Deconvolution were used. Images were taken with ZEN black software, cropped with Adobe Photoshop CS6 and designed with Adobe Illustrator CS6. Three-dimensional reconstruction were received with Imaris 8.2 and projections with ZEN 2.3.

2.3. Quantitative Real-Time PCR (qRT-PCR)

Precisely staged larvae were collected and frozen in lysis buffer at −80 °C. Larvae were lysed using the Precellys homogenizer (Peqlab) and RNA was extracted using the NucleoSpin RNA II Kit (Macherey-Nagel, Düren, Germany) following the manufacturer's instructions. 500 ng RNA was subjected to cDNA synthesis using the QuantiTect Reverse Transcription Kit (Qiagen, Hilden, D). qRT-PCR was carried out as described in (Pesch et al., 2015) with a CFX96 cycler (Bio-Rad, Munich, D). All qRT-PCR reactions were carried out with at least five biological replicates and standard control PCR reactions (negative control, no template control) were used to rule out contaminations. For normalization transcript levels of *rp49* (Ribosomal protein L32) were used. As a control *obst-A* mutant larvae were tested for the absence of *obst-A* expression (Petkau et al., 2012). All primers were tested for potential dimer formation as well as for their efficiency. Primer sequences and efficiencies are depicted in Supplementary table S1. Significance was tested using one-way ANOVA and multiple *t*-tests (Graph Pad Prism 6) and p-values are indicated by asterisks (* $p < 0.05$, ** $p < 0.01$, ***$p < 0.001$). Error bars indicate the standard error of the mean (SEM).

2.4. Pull down assays

For Glutathione-S-transferase (GST) experiments, Wurst large extracellular loop was expressed in fusion with a GST Tag to allow purification by GST-beads and pull-down assay. Primers: GGCGGCACTGACCTTCGA, CCAGAAGGCGCAGTAGAT; The predicted large extracellular loop of the Wurst protein is located between the fifth and sixth transmembrane domains. For construct and primer details see supplement. PCR products were cloned by EcoRI and Xho1 restriction into the GST 4T3 vector. GST-Wurst-domain fusion proteins were purified with Sephadex 4b (Amersham) at 4 °C for 1 h and tested by coomassie brilliant blue stainings at control SDS gels and by additional Western Blot analysis using anti-GST antibody. Pull down assays were performed as previously described (Petkau et al., 2012). The antibody specifically detects Obst-A as previously shown (Petkau et al., 2012) and was used at a 1:5000 dilution.

3. Results

3.1. Obst-A is required for the control of ecdysteroidogenic genes

A typical set of phenotypes has been described as characteristic of mutations that affect ecdysone signaling, such as larval arrest, growth size defect and retained cuticles (Gates et al., 2004; Gaziova et al., 2004; Li and Bender, 2000; Ou et al., 2016; Perrimon et al., 1985; Yamada et al., 2000; Yoshiyama et al., 2006). Given that *obst-A* null mutant first instar larvae display all of these phenotypes (Petkau et al., 2012), we asked whether Obst-A has any impact on the expression of genes required for ecdysone production. The investigated ecdysone pathway and important downstream targets are summarized in the supplement (Fig. S1A). We investigated expression levels of fifteen representative genes of the ecdysone machinery. This was addressed by performing quantitative real-time PCR (qRT-PCR) at five different time-points, covering the entire first instar development. Three time-points were chosen to exclusively monitor late first instar development shortly before and during molting when ecdysone levels should rise. To summarize, in *obst-A* mutant first instar larvae RNA levels of all fifteen analyzed genes involved in the ecdysone machinery remained significantly lower when compared to wt and did not show any pulsatile up-regulation (Fig. 1A; Fig. S1B). In contrast in wt animals eleven genes showed a clear pulse-like upregulation (*neverland, spookier, shade, phantom, EcR, ftz-f1, E74A, cyp18a, eh, eth*) in late first instar development. Their RNA levels increased only shortly before ecdysis and declined few hours later at the end of transition to second instar larvae (Fig. 1A; Fig. S1B). Only the co-receptor gene *ultraspiracle (usp)* was expressed at rather constant levels in wt (Fig. S1B). Additionally, the *broad complex* genes and *shroud* RNA levels were at highest levels at the beginning of first instar development in wt, which has been previously described in part (Niwa et al., 2010). Importantly, the early response gene *E74A* as a direct target of the active ecdysone machinery becomes ~150 times up-regulated in wt larvae. This very strong rise of RNA levels was completely absent in *obst-A* mutants (Fig. 1A). In summary, these findings provide evidence that, in contrast to wt, genes of the ecdysone machinery and peripheral target hormones failed to be up-regulated in late first instar *obst-A* mutants.

In case of defective ecdysteroidogenesis, feeding specific types of ecdysteroids can rescue molting defects and ecdysis into the next larval stages (Danielsen et al., 2014; Niwa et al., 2010; Yoshiyama et al., 2006). To restore first instar lethality *obst-A* mutants larvae were fed either with cholesterol or 7-dehydrocholesterol (7dC), both are substrates in the ecdysone biosynthesis pathway, or with two different concentrations of the active molting hormone 20E. The non-treated *obst-A* mutant larvae served as control and died as late first instar larvae during molting. Upon feeding with ecdysteroids, a small but significant number of *obst-A* mutant larvae died after partial molt or molt into second or even third instar stage with the tendency that the higher concentrations of 20E showed best results (Fig. S1C). To circumvent the strong lethality associated with the loss of *obst-A* due to Obst-A function in trachea and epidermis (Pesch et al., 2015; Petkau et al., 2012), the feeding experiment was repeated in 69BG4 driven *obst-A* RNAi-mediated knockdown animals. This showed a significant rise in the number of animals that survived to adulthood upon ecdysteroid feeding (Fig. S1D). Collectively, qRT-PCR and feeding data demonstrate that Obst-A supports 20E production and thereby the ecdysone machinery for larval molting. We next addressed whether the nuclear localization of the Ecdysone Receptor (EcR) itself (Johnston et al., 2011) is under control of Obst-A. Late first instar control larvae revealed cytoplasmic but predominantly nuclear staining of EcR in the dissected ring glands and surrounding tissues (Fig. S1E). In the corresponding *obst-A* mutant larvae EcR staining showed a similar pattern, indicating that Obst-A- is not involved in nuclear EcR localization which controls ecdysone signaling events.

Ventral veins lacking (Vvl), Knirps (Kni), Molting defective (Mld) and Without children (Woc) are transcription factors required for expression of genes regulating ecdysone biosynthesis in the endocrine PG cells (Danielsen et al., 2014; Uryu et al., 2018; Warren et al., 2001). Their gene activity profile in first instar was assessed by qRT-PCR. All four genes showed highest RNA levels at the first half of first instar development in control animals but significantly lower levels in *obst-A* mutants (Fig. 1B). In addition, *vvl* and *kni* are also required to maintain PTTH hormone signaling, which is the major signal for ecdysteroid synthesis in PG cells (Danielsen et al., 2014). *ptth* RNA levels were reduced in the *obst-A* mutant during beginning of first instar development and remained at low levels in late first instar larvae when compared with control animals (Fig. 1B). These findings indicate that even early factors, which influence the activation of genes for ecdysteroid production were affected upon loss of *obst-A* (summarized in Fig. 1B).

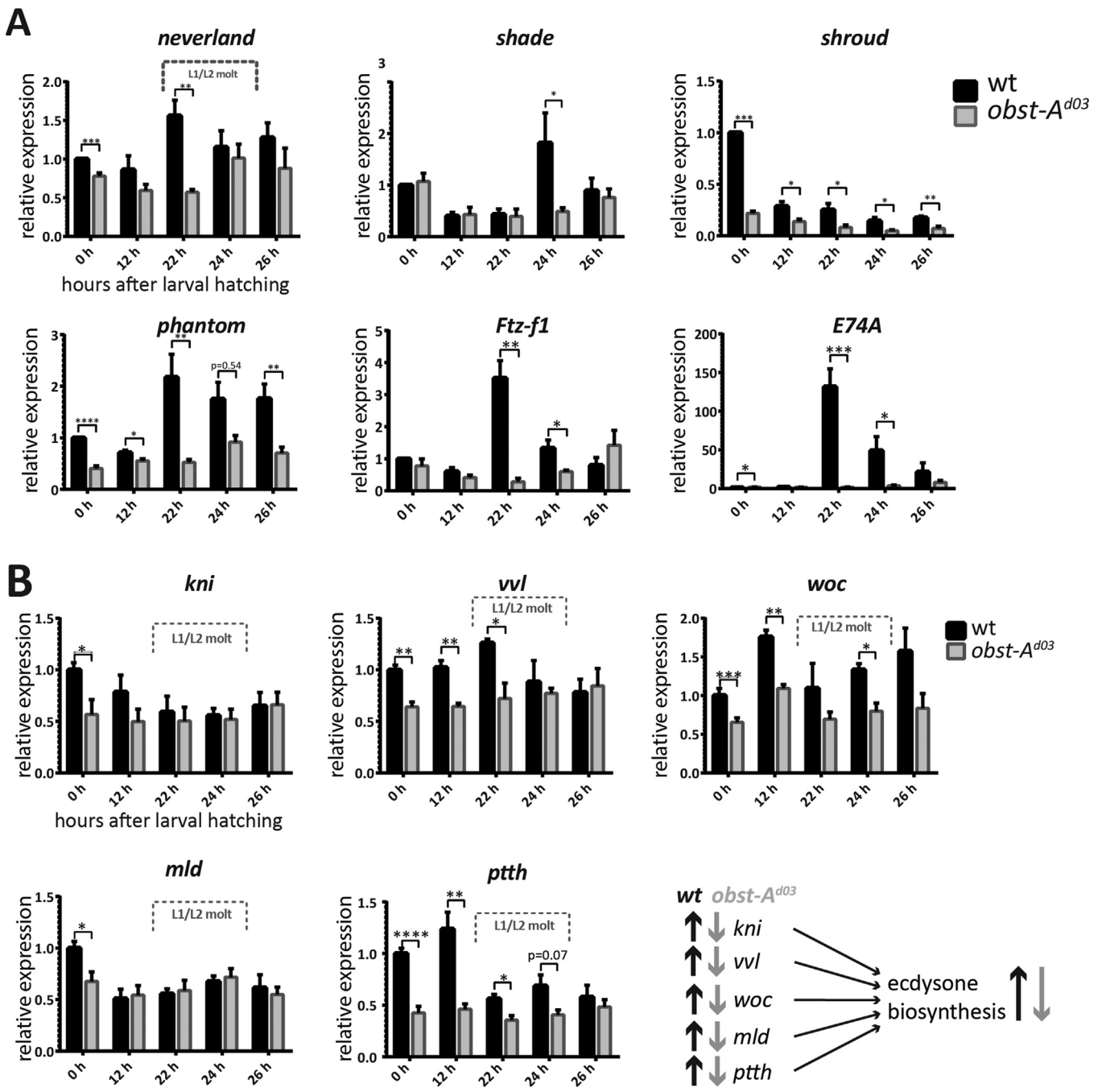

Fig. 1. Control of genes involved in the ecdysone biosynthesis machinery depends on Obst-A. (A) qRT-PCR analysis of relative RNA expression of representative ecdysteroidogenic genes in first instar larvae; triplicates and n = 5 independent experiments (hours after larval hatching). Error bars represent Standard error of mean (SEM); p-values are represented by asterisks: * $p < 0.05$, ** $p < 0.01$, *** $p < 0.001$. All qRT-PCR reactions were carried out of at least five biological replicates. (B) qRT-PCR analysis of relative RNA expression of *kni, vvl, woc, mld* and *ptth* in first instar larvae (hours after larval hatching). SEM is indicated by lines, p-values are represented by asterisks: * $p < 0.05$, ** $p < 0.01$, *** $p < 0.001$. Summary of results of RNA levels in control (black arrows) and *obst-A* mutant (grey arrows) larvae and role of transcription factors in the PG.

3.2. Obst-A defines the extracellular matrix of ecdysone producing PG cells

Recently, it has been shown that two cerebral tracheal branches, one per hemisphere, grow dorsally from anterior towards posterior, contacting the embryonic PG cells of the ring gland (Sánchez-Higueras and Hombría, 2016). In stage 16 embryos Obst-A is expressed in both cerebral branches and in the PG cells that are in contact with (Fig. 2A). In stage 16 *obst-A* null-mutant embryos Obst-A staining was not detectable in trachea or PG cells (Fig. 2B) demonstrating Obst-A antibody specificity for PG staining. Interacting with the PG, cerebral tracheal branches contribute to ring gland migration efficiency during second half of embryogenesis (Sánchez-Higueras and Hombría, 2016). At embryonic stage 14 the ring gland is formed as a V-shaped structure containing both CC at the central part which are attached on each side to the PGs. The PGs connect distally to the CA (Sánchez-Higueras and Hombría, 2016). Since the PG associated cerebral tracheal branches secrete Obst-A from stage 14 onwards, we were curious whether tracheal Obst-A contributes to PG formation. To test this we generated tracheal-specific UAS-*obst-A*-RNAi knockdown embryos using the strong tracheal driver line *breathless* (*btl*)-Gal4 line. The resulting embryos revealed tracheal specific Obst-A knockdown while PG lobes showed normal Obst-A staining. Thus, PG specific Obst-A expression was independent from tracheal cells. Further, tracheal obst-A knock-

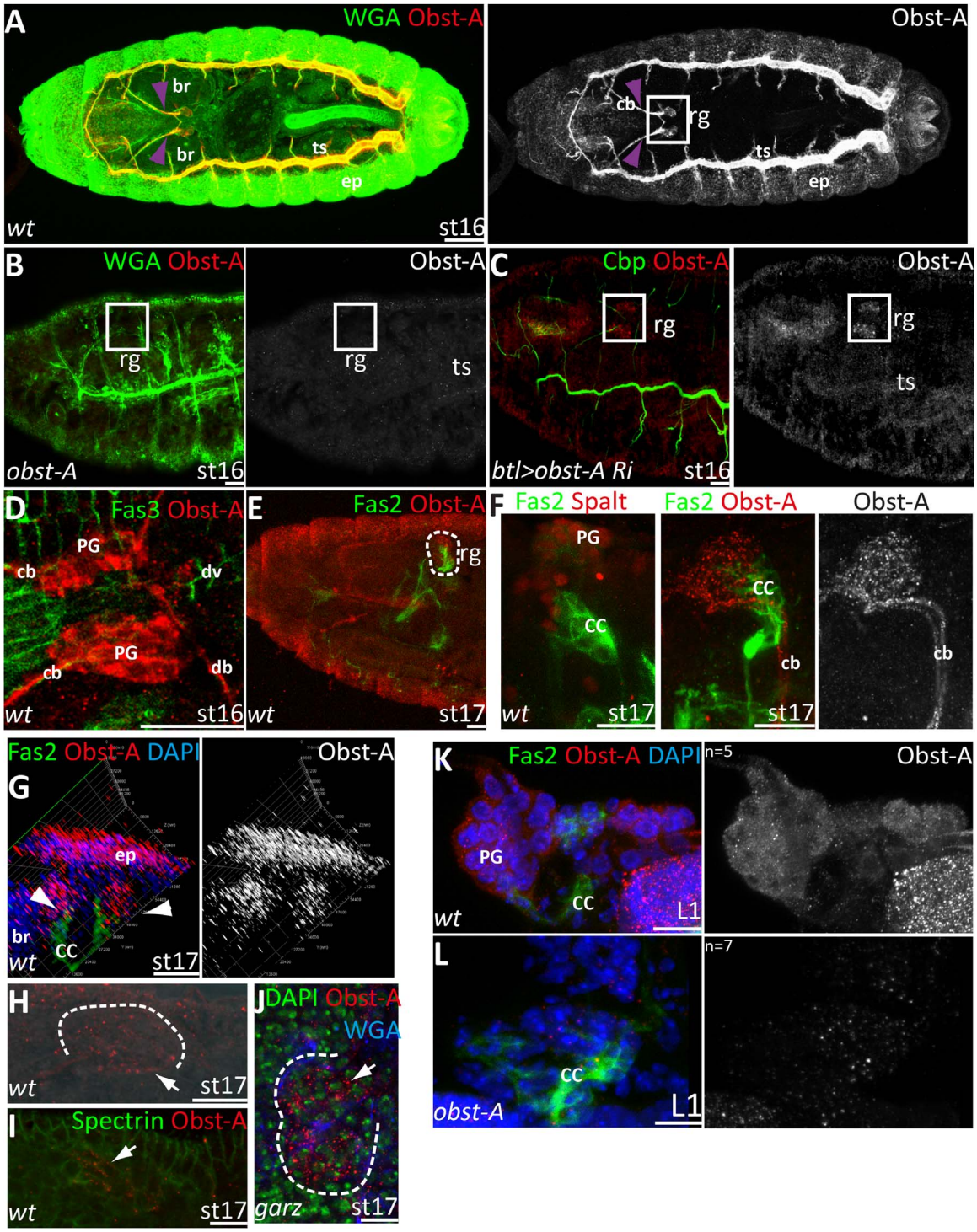

Fig. 2. Obst-A is expressed in PG cells of embryos and larvae which is independent from its tracheal expression. Confocal analysis of a whole mount embryos and larvae. (A) Projection of a stage 16 embryo (anterior left, dorsal view) shows Obst-A (red) expression in the tracheal system (ts), the epidermis (ep) and the ring gland. WGA (green) labels cell surfaces including chitinous structures. Purple arrowheads point to the two cerebral tracheal branch (cb), one each hemisphere, reaching dorsally to the PG cells (Sánchez-Higueras and Hombría, 2016). Single Obst-A channel is indicated in grey. Obst-A is expressed in the cerebral tracheal branches and the contacted ring gland (white frame); (B) In stage 16 hemizygous *obst-A* null mutant embryos Obst-A staining is not detectable (white frames indicate ring gland); n = 5. (C) *btl*-Gal4 driven *obst-A* RNAi knockdown (n = 8 embryos) showed reduced Obst-A staining in the tracheal branches but normal expression in the ring gland. Chitin binding probe (Cbp, green) detects chitin in the tracheal lumina. Shape and localization of ring glands (frame) were indistinguishable between knockdown and wt embryos. (D) Stage 16 *wt* embryos reveal Obst-A staining in the PG cells (dorsal view) next to the vessel (dv) expressing Fas3 (in green). (E,F) Stage 17 *wt* embryos reveal Fas2 (green) expression in the CC and Spalt (red) and Obst-A (red) expression in the PG (lateral view). Single Obst-A channel is indicated in grey. (G) Three-dimensional reconstructions show stage 17 *wt* embryo ring gland located underneath the dorsal epidermis (view from anterior). Obst-A (red) staining overlaps dorsally with Fas2 (green) marked CC of cells the ring gland (arrows point to the Obst-A staining of PG). Nuclei are stained in blue with DAPI. (H) Stage 17 wt embryos stained with Obst-A (red). Single imaging taken with a spinning disc confocal and combined with brightfield microscopy, reveals Obst-A accumulation at the border of PG lobes (encircled by white dashes, arrow). (I) Spinning disc image shows Obst-A (red) overlap (arrow) with α-Spectrin (green) at the PG membranes in wt stage 17 embryos. (J) Confocal images of stage 17 *garz* mutant embryo reveals Obst-A (red) accumulation (arrow) next to DAPI (green) at PG cells. WGA (blue) marks cell membrane surfaces and nuclei membranes. (K,L) First instar larvae show Obst-A (red) expression in the PG (H), while in *obst-A* null mutant larvae Obst-A was not detectable in the PG. Fas2 (green) labels CC cells and DAPI (blue) the nuclei. br, brain; cb, cerebral tracheal branch; db, dorsal branch; dv, dorsal vessel; ts, tracheal system; fg, foregut; ep, epidermis. CA, corpora allata; CC, corpora cardiaca; PG, prothoracic gland. Anterior is left. Scale bars indicate 50 μm for whole mount embryos in A and 10 μm for all other images.

down embryos revealed normal localization of PGs underneath the dorsal epidermis and connected with the two cerebral tracheal branches (Fig. 2C).

Next we addressed Obst-A expression and its subcellular localization in the ring gland. In order to release ecdysone into the hemolymph, PGs cells contact the anterior part of the *Drosophila* circulatory system, termed as dorsal vessel (Yamanaka et al., 2015). Indeed, PG specific Obst-A staining was found next to Fas3, which detects the dorsal vessel cells (Johnson et al., 2011) (Fig. 2D). Fasciclin (Fas)2 labels the CC and CA cells (Fig. 2E) while Spalt detects nuclei of PG cells (Barrio et al., 1999; Sanchez-Higueras et al., 2014). Immunofluorescent Spalt and Obst-A stainings showed similar expression pattern labeling PG cells with regard to the adjacent Fas2 positive CC cells (Fig. 2F). However, Obst-A staining was not observed in CC cells. In late embryos when the transient V-shaped structure of the ring gland (Sánchez-Higueras and Hombría, 2016) is generated the CA continue their dorsal migration and fuse to each other forming a ring-like structure (Sánchez-Higueras and Hombría, 2016). This structure is present from embryo stage 16 onwards around the anterior end of the dorsal vessel (Hartenstein, 2006). Three-dimensional projections revealed late embryonic ring-like shape of the ring gland where Obst-A staining was detected in the PG lobes dorsally to Fas2 positive CC cells, and underneath the epidermis (Fig. 2G). Brightfield images show Obst-A accumulation at the border of PG lobes (Fig. 2H), indicating that Obst-A could be localized at or next to the membrane. This was supported by Obst-A overlap with α-Spectrin, labeling the membrane skeleton of PG cells (Fig. 2I). Consistent with its possible extracellular localization, Obst-A secretion was prevented in *gartenzwerg* (*garz*) mutant embryos, which leads to insufficient transport of apical proteins and membrane components (Wang et al., 2012). In *garz* mutants, Obst-A accumulated predominantly next to nuclei as marked by DAPI (Fig. 2J). Further, dissected first instar ring glands showed strongest Obst-A staining in the PG and CA, while *obst-A* null mutant larvae of the same age did not show Obst-A staining demonstrating antibody specificity also for larval stainings (Fig. 2K,L). Collectively, our findings provide evidence that Obst-A is expressed in the PG cells where it is predominantly localized at cell surfaces.

3.3. Obst-A is not required for cell proliferation of PG cells

Next, we addressed whether Obst-A has any impact on the ring gland morphology in late embryos. Using Spalt as a marker for PG cells, where Obst-A is expressed from stage 16 onwards, we did not observe any obvious difference between late wt and comparable *obst-A* mutant embryos. All embryos showed nuclear Spalt expression and no obvious changes in size and number of PG cells (Fig. 3A). This was further confirmed by analyzing cell cycle progression. Recently it was shown that the PG size is controlled by Aurora-A, an essential guardian of cell cycle progression (Vaufrey et al., 2018). Histone H3 is phosphorylated at Ser-10 by Aurora-A kinase activity during mitosis and meiosis in a wide range of organisms (Hsu et al., 2000). Using an antibody that detects the phosphorylated Histone H3, we did not observe any difference between wt and *obst-A* mutant embryos (Fig. 3B). These findings argue that cell cycle progression and overall PG morphology appear normal in late *obst-A* mutant embryos.

3.4. Obst-A is required for axon formation at PG cell matrix

Fas2 is the *Drosophila* ortholog of neuronal cell adhesion molecule (NCAM) and specifically labels CC and CA cells, as well as axons innervating the ring gland. Despite Fas2 positive nerves that terminate in the CC, other Fas2 positive axons continue dorsally and terminate in the CA, previously referred to as axons to the corpus allatum (aca) (Velasco et al., 2007, 2004). A role of Fas2 positive axons in regulating PG activity has not been demonstrated, but due to the pattern, we used Fas2 as a well-established marker for analyzing CC, CA and axons at the ring gland. Ring gland morphogenesis involves axon growth at its surface. We dissected the small ring glands of late first instar larvae and stained those with Fas2 antibody in combination with WGA (wheat germ agglutinin), a lectin that detects sugar residues at cell surfaces, and with DAPI. Analysis of Z-stacks and three-dimensional reconstructions resulted in the visualization of the entire ring gland, their extracellular surfaces and cell nuclei. As expected, control larvae showed Fas2 positive CC and CA, and Fas2 positive axon-like structures that continue dorsally along the PG surface towards the CA (Fig. 3C). The two large PG lobes were recognizable by large nuclei size at the ring gland. In contrast, all *obst-A* null mutant larvae lacked characteristic Fas2 positive axon-like structures at the PG surfaces (Fig. 3D).

In dissected late first instar larval ring glands, co-immunostainings revealed distributed extracellular Obst-A staining at PG cells that also surrounded Fas2 axon-like structures in a punctuate pattern. Surface rendering and orthogonal projections of confocal Z-stacks indicated that Obst-A staining coated the PG surface where Fas2 stained axons exist (Fig. 3E). This prompted us to address if there is a PG specific requirement of Obst-A and a time specific correlation between Obst-A and Fas2 expression at the ring gland surfaces. This was assessed by knocking down *obst-A* predominantly in the PG cells using the Mai60-Gal4 driver (Walker et al., 2013). We used Mai60-Gal4 because other PG driver lines were very weak in embryos and L1 larvae, such as P0206-Gal4 and phantom-Gal4 (own observation). Additionally, the 69B-Gal4 driver line was used to generate a general, but mild knockdown since it is active in all Obst-A expressing organs including the ring gland (Gal4 drivers are summarized in Fig. S2A). The driver-line specific *obst-A* knockdown was evaluated by qRT-PCR and immunostainings using the Obst-A specific antibody. In Mai60-Gal4 and 69B-Gal4 driven knockdown experiments *obst-A* RNA levels and Obst-A staining in the ring gland of late embryos was strongly reduced compared to wt (Fig. S2B,C). Confocal images addressed PG shape and Fas2 expression in late *obst-A* knockdown embryos. The V-shape appearance of the CC found in wt embryos and visualized with Fas2 staining, was not affected by *obst-A* knockdown or altered in *obst-A* mutants, but *obst-A* null mutant as well as PG specific Mai60-Gal4 and 69B-Gal4 driven *obst-A* knockdown embryos lacked Fas2 positive axon-like structures at the surface of PG cells. This resembles the phenotype observed in *obst-A* mutant first instar larvae (Fig. 3D, Fig. 4A, Fig. S3A). By contrast, first instar wt larvae and stage 17 control embryos possessed Fas2 positive axon-like structures reaching dorsally at the PG surface probably towards the CA (Fig. 4A; Fig. S3A). These findings indicate that Fas2 positive axon-like structures at the PG surface were compromised upon both lack and reduction of PG specific Obst-A surface expression (Fig. 3F).

To further address the temporal relationship between Obst-A expression and Fas2 appearance at the ring gland co-immunostainings were performed in late embryos. WGA was used as an extracellular surface marker. PG specific Obst-A expression starts in late stage 16 when constrictions of the four midgut lobes become visible. During this time range, Fas2 positive axon-like structures appeared at the PG surface (Fig. 4B-C‴). Higher magnifications showed Obst-A staining in a punctuate pattern distributed at the PG surface of late stage 16 and stage 17 embryos (Fig. 4D-D′). Deconvolution of confocal images showed that Obst-A overlapped with Fas2 positive axon-like structures and with the fine branches that sprouted out from the observed axons at the PG surface of late stage 16 embryos (Fig. 4E,F). The positive correlation of observed Obst-A and Fas2 stainings at the PG surface is presented in a schematic model (Fig. 4G). This led to the question of how Obst-A could impact axon growth at the PG surface. In tracheal and epidermal cells Obst-A regulates chitin-matrix packaging and maturation thereby promoting cuticle stiffness and integrity. Even slight mechanical stresses, such as touching or gentle pricking of *obst-A* mutant larvae led to epidermal burst and organ spill out, indicating the importance of Obst-A for keeping epithelial resistance during wound repair (Petkau et al., 2012). Since axons grown on stiff substrates are

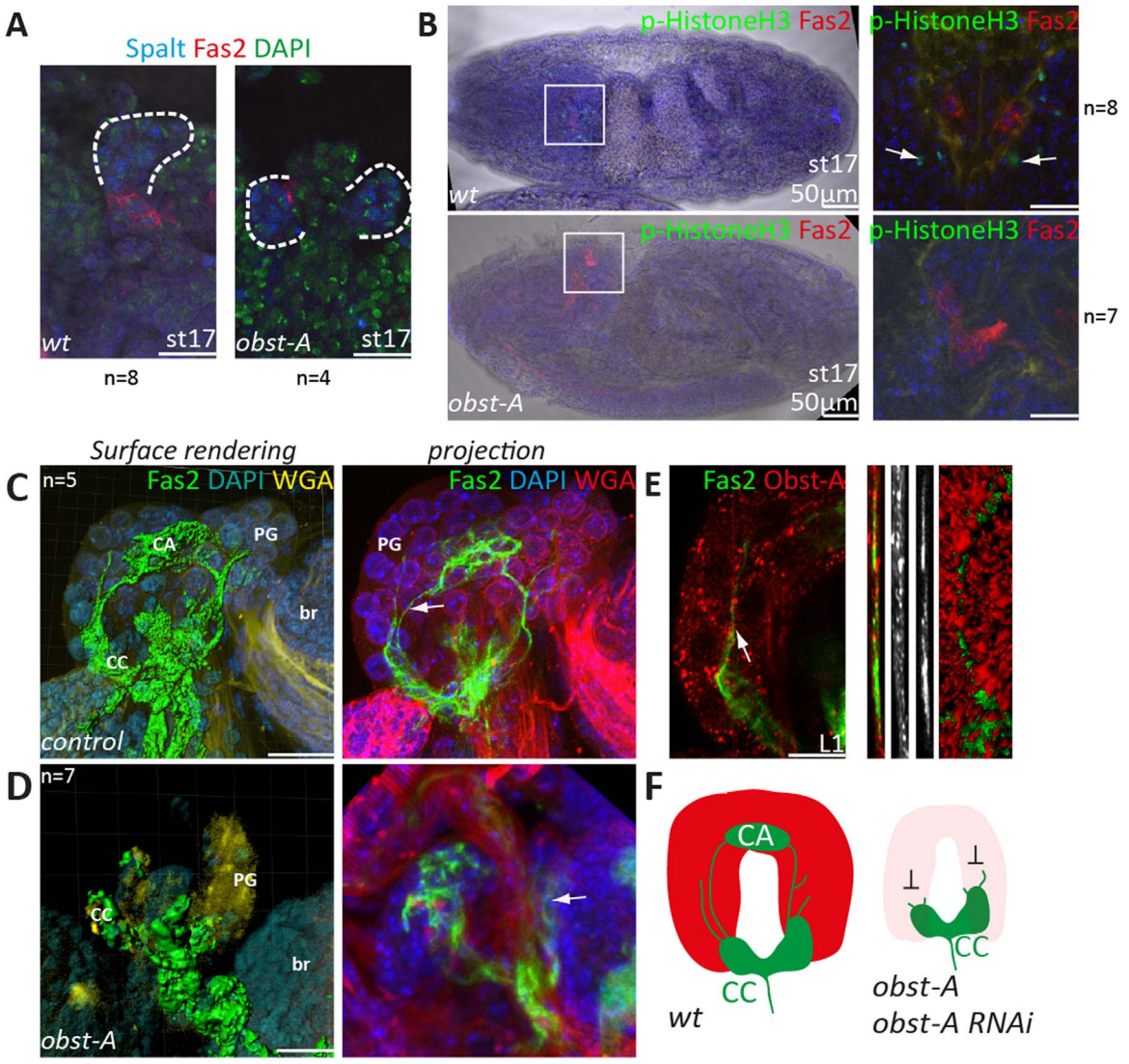

Fig. 3. Obst-A is required at the extracellular surface of PGs but is not involved in cell cycle progression. (A) Spalt (blue) expression in the PG cells (encircled by white dashes) next to Fas2 (red) labeled CC in *wt* (left view of PG lobe) and *obst-A* mutant (dorsal view, both PG lobes) st 17 embryos is indistinguishable. DAPI was used to detect nuclei (green). (B) Phospho-Histon H3 (green) expression was detected neither in wt (dorsal view) nor in *obst-A* mutant (lateral view) ring gland cells (white frame), but in neighboring tissue cells (arrows), in stage 17 embryos. Fas2 was used to detect the CC (red). DAPI (blue) detects nuclei. Overview (left image), magnifications of the ring gland (right image). (C,D) Three-dimensional reconstruction (left hand) of confocal Z-stacks and confocal maximum intensity projection (right hand) showing the first instar ring gland marked with Fas2 (green), DAPI (blue) and WGA (yellow and red). Note the Fas2 positive axons projecting dorsally at the PG cells towards CA and axon-like structures ending at the PG (arrows in B, left image) (n = 4). In *obst-A* mutants (right images) such Fas2 positive axon-like structures were not found at the PG or appear misrouted (arrow in B, right image). (E) Single confocal image and orthogonal projections of Z-stacks (left three images) and the surface reconstitution (right image) indicate the how Obst-A surface staining surrounds Fas2 axon-like structures running at the PG. Red line (arrow) in the left hand image indicates where the orthogonal projection was generated. (F) Schematic drawing summarizes formation of Fas2 positive axons (green) in control embryos and larvae versus *obst-A* mutant and knockdown animals. Scale bars represent 10 µm if not otherwise indicated.

significantly longer than those on soft substrates (Koser et al., 2016), the abolishment of Fas2 axon-like structures in *obst-A* mutants could be caused by a less stiff PG cell surface, analogous to the soft *obst-A* mutant cuticle. To exclude in this context the probability that Obst-A acts as a chemoattractant (Kruger et al., 2005), we performed Obst-A overexpression. However, neither Mai60-Gal4 nor 69B-Gal4 driven Obst-A overexpression in the PG and ring gland cells, respectively, caused unusual extra sprouting or misrouting of Fas2 positive axon-like staining at the PG surface (Fig. 4H,H′; Fig. S3B).

As Obst-A can determine PG surface properties analogous to its function in the cuticle, this raises the question whether other cuticle proteins and enzymes, interacting with Obst-A, may play a role at the PG surface. In the cuticle Obst-A recruits the chitin-protector Knickkopf (Knk), and the deacetylases Serpentine (Serp) and Vermiform (Verm), to the growing chitin-matrix (Pesch et al., 2015). To this end we performed expression analysis in wt embryos, but neither chitin, nor Knk, Serp or Verm were found at the ring gland surfaces (Fig. S4 A-D). This was further confirmed by Mai60-Gal4 driven PG knockdown of *knk*, which did not cause larval lethality, retained cuticles, or any other known ecdysone deficient phenotypes (Fig. S4E). Thus, PG matrix is devoid of chitin and known associated proteins, suggesting that Obst-A function at the ring gland surface is independent from chitin and so far is unique among the large number of known cuticle and chitin binding proteins.

3.5. Obst-A expression in the PGs is required for larval survival and growth control

Finally we addressed the biological consequences of Obst-A function at the ring gland surfaces. This was assessed by ring gland specific *obst-A* knockdown in the CC (*akh*-Gal4), the PG (Mai60-Gal4), and the CA (aug21-Gal4) cells. In addition we tested *obst-A* knockdown in *ptth*

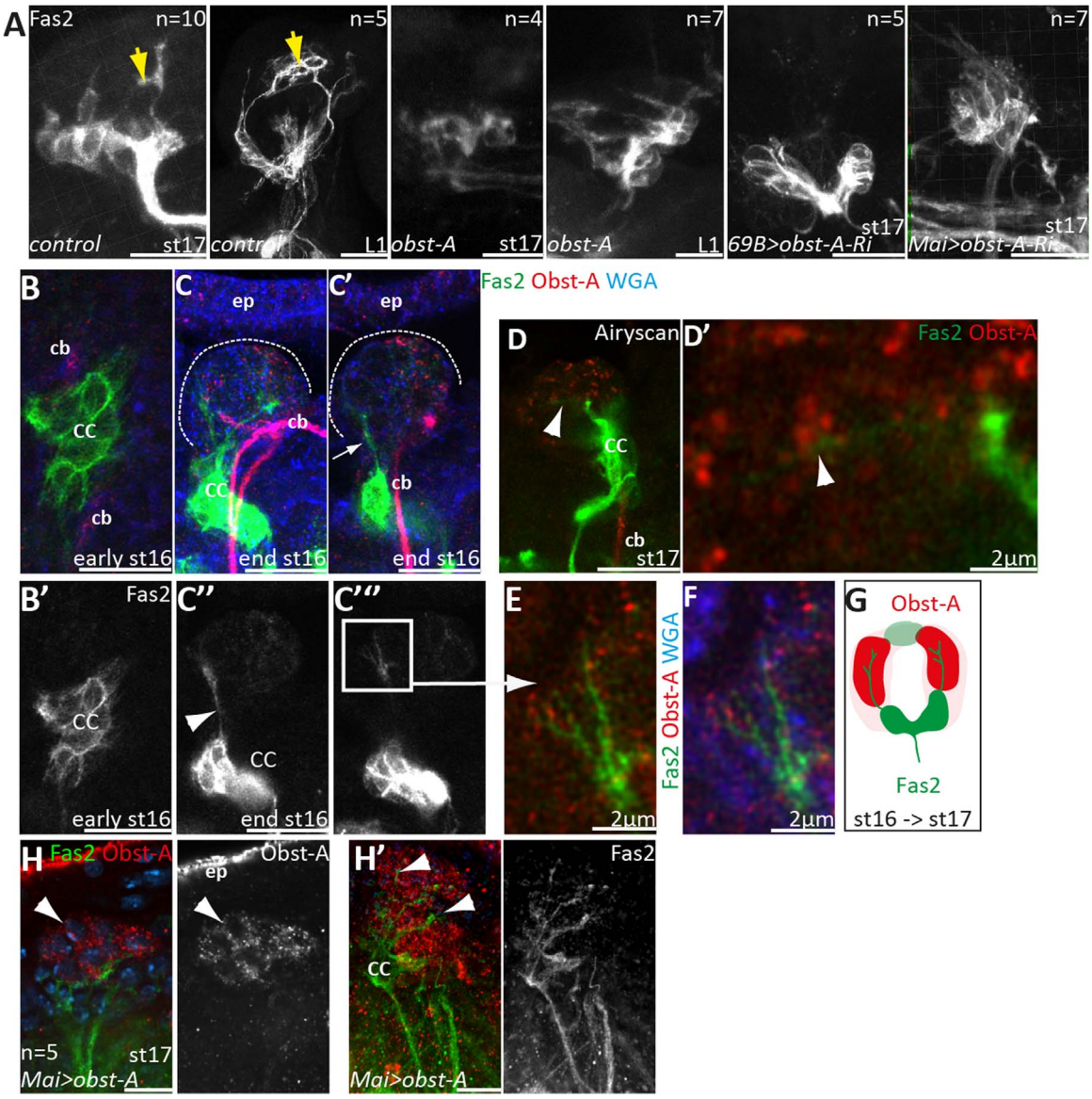

Fig. 4. Extracellular Obst-A is substantial for Fas2 positive axon structures at the PGs. (A) Three-dimensional projections (ring glands from anterior view) of st17 embryo and first instar (L1) show Fas2 positive CC cells and Fas2 positive axon-like structures (yellow arrows) projecting dorsally at the PG towards the CA (Velasco et al., 2007). The *obst-A* mutant stage 17 embryo, first instar larvae and 69B-Gal4 and Mai60-Gal4 driven *obst-A* RNAi mediated knockdown mutants show impaired Fas2 positive axon-like structures formation at the PG surface. Multiple color channels are presented in Fig. S3A. (B-C‴) Early stage 16 wt embryos (before three midgut constrictions appear) showed only Fas2 (green) at the CC. Additional Fas2 positive axon-like structures (arrow in C′) were detectable at later stage 16 (when three midgut constrictions are present) when also Obst-A (red) appeared at the PG surface. B,C show confocal projections and C' confocal image. Single Fas2 channels are indicated in the panel below in grey WGA is presented in blue. (D,D′) Confocal AiryScan images show Obst-A (red) staining in a punctuate pattern distributed at the PG surface overlapping with Fas2 (green) labeled axon-like structures. (E,F) During late stage 16 Fas2 (green) positive axon-like structures show fine branches at their dorsal end. These overlap with Obst-A (red) puncta at the PG surface, marked by WGA (blue). (G) Schematic model indicates positive correlation of Fas2 (green) staining and Obst-A (red) distribution at the PG surfaces. (H,H′) PG specific Obst-A overexpression in Mai60-Gal4 UAS-Obst-A stage 17 embryos show Fas2 (green) positive axon-like structures at the PG. DAPI (blue) detects PG nuclei. Obst-A single channel is indicated in grey. Spinning Disc images (H) and Z-stack projection (H′). cb, cerebral tracheal branch; CC, corpora cardiaca; PG, prothoracic gland. Scale bars represent 10 µm.

expressing neurosecretory cells (*ptth*-Gal4). The *obst-A* knockdown in CC, CA and *ptth* cells did not cause lethality or any other ecdysone deficiency phenotype (Fig. 5A; Fig. S3C). In contrast, the PG specific Mai60-Gal4 *obst-A* RNAi-mediated knockdown caused a wide a range of severe phenotypes resembling *obst-A* null mutant and ecdysone deficient mutants. Reducing Obst-A at the PG surface resulted in lethality at the transition from first to second instar. Knockdown animals that survived for a couple of days arrested in body size at the ecdysis to second instar and showed typical molting defects (Fig. 5B,C). Collectively, these findings summarize the essential role of Obst-A at the extracellular surface of ring gland PG cells,

However, this leaves the question whether PG expression of Obst-A is sufficient to rescue lethality at transition from first to second instar stages. We therefore re-expressed Obst-A within the ring gland of *obst-A* null mutant larvae by using Mai60-Gal4. Although Obst-A function in the exoskeletal cuticle is very essential (Pesch et al., 2015), 12% of such animals survived larval transitions and molted to pupae (Fig. S5A,B). Interestingly, they showed deformed body shape (Fig. S5C), reminiscent of *obst-E* mutants where cuticles fail to undergo shape changes (Tajiri et al., 2017).

Curious as to whether Obst-A could also play a role during later larval development, we knocked down Obst-A in late larval stages using two different Gal4 lines. It was reported that P0206-Gal4 is expressed moderately throughout PG and strongly in the CA and Aug21-Gal4 is expressed in the CA and salivary glands (Mirth et al., 2005). We observed that P0206-Gal4 as well as Aug21-Gal4 driven *obst-A* RNAi

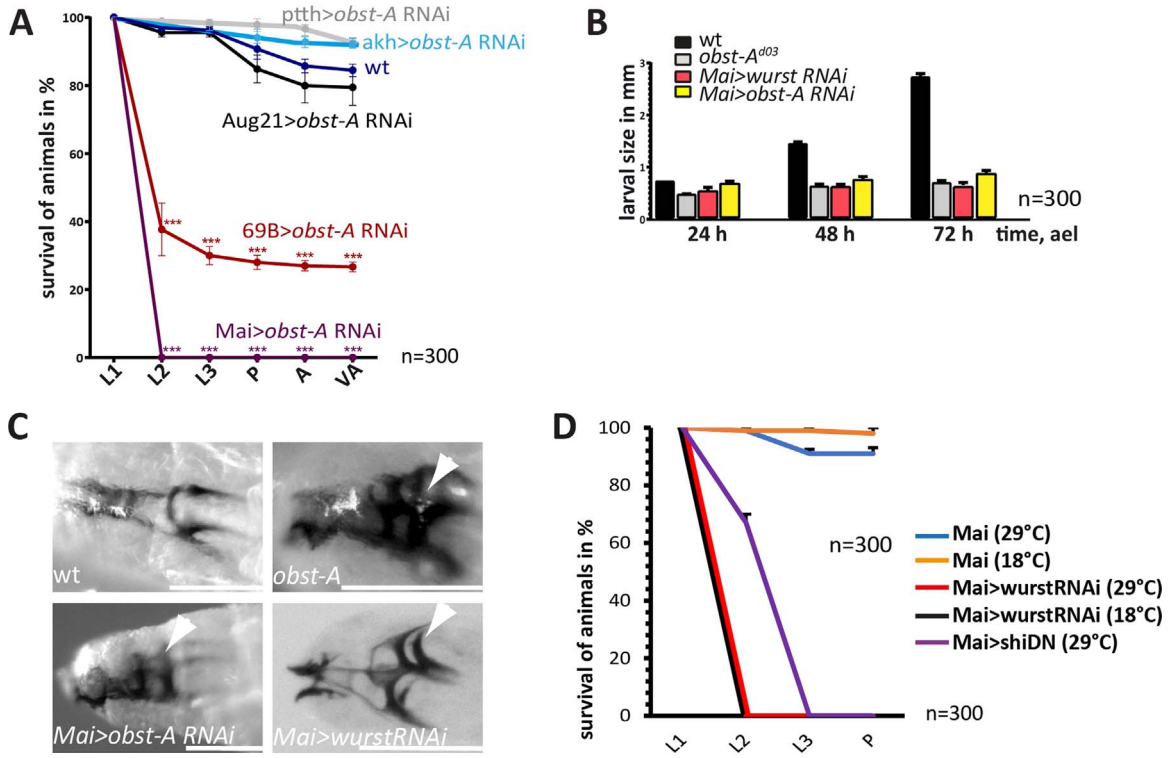

Fig. 5. PG specific *obst-A* and *wurst* knockdowns caused larval death, molding defects and growth arrest. (A) Histogram indicates survival of control and of Mai60-Gal4, 69B-Gal4 Aug21-Gal4, ptth-Gal4, akh-Gal4 driven *obst-A* (n = 300 each) knockdown animals in percentage monitored throughout development. Standard deviations are indicated by lines. p-values are represented by asterisks: * $p < 0.05$, ** $p < 0.01$, *** $p < 0.001$. (B) Graph indicates body size in mm of control (black), *obst-A* null-mutants (grey) and PG specific (Mai60G4) *obst-A* and *wurst* knockdown animals at 0 h, 24 h and 48 h after larval hatching. N = 300. (C) PG specific Mai60-Gal4 driven *obst-A* and *wurst* knockdown caused molting defects (arrows point to unusual double cuticles) in late first instar larvae that failed to shed off old cuticles, resembling *obst-A* null mutants. (D) Histogram shows survival of control and of PG specific Mai60-Gal4driven *wurst* knockdown and *dynamin (*UAS-shi^{DN}*)* dominant negative mutant animals in percentage throughout development. Experiments were performed at 18 °C and 29 °C; n = 300 for each genetic condition.

knockdown larvae were developmentally delayed, molted to L3 later than wt and control larvae. For staging larvae independently from time points after egg laying (AEL), we analyzed morphology of anterior and posterior spiracles (Vaufrey et al., 2018). By day three (72 h AEL) 96% (n = 100) of the wt (and also other controls) molted to third instar. In contrast, only 24% (P0206-Gal4 driven) and 20% (Aug-21-Gal4 driven) *obst-A* knockdown molted to third instar while all other larvae remained as L2-stage. Furthermore, in contrast to delayed L2-stage, knockdowns were extremely fast through L3-stage, molted to pupa even before wt and control animals. By five days (120 h AEL) 42% of the wt versus > 90% of the knockdowns molted to pupa (Fig. S6A,B). Potential Obst-A roles during late larval development were supported by immunostainings showing Obst-A expression in the third instar ring gland (Fig. S6C).

3.6. Endocytosis controls extracellular Obst-A localization and axon formation at the PGs

Axonal growth requires continuous membrane expansion but also extracellular cues to regulate motility (Araujo and Tear, 2003; Nozumi et al., 2017). Dynamic changes of nerves are under control of local endocytic internalization processes (Tojima et al., 2010). Although Obst-A punctuate staining shows only partial overlap with Clathrin heavy chain (Chc) in embryonic ring gland PG cells (Fig. S3D), it suggests that extracellular Obst-A could be internalized via Clathrin vesicles. Wurst (orthologous to human DNAJC22), a transmembrane J-domain protein that recruits clathrin heavy chain (Chc) to the membrane, mediates endocytosis of tracheal cuticle proteins (Behr et al., 2007; Stümpges and Behr, 2011). Immunostainings show typical punctuate Wurst pattern distributed in the Spalt positive PG cells of late embryos (Fig. 6A). At the subcellular level Wurst vesicle-like punctuate staining (Behr et al., 2007) overlapped with Fas2 positive cells and axon-like structures (Fig. 6B). Co-immunostainings also showed partial overlap of Wurst vesicles with Obst-A and the Fas2 positive axonal staining (Fig. 6C). In GST- pull down assays using the extracellular Wurst domain, Obst-A precipitated from embryo extract (Fig. 6D). The blockage of endocytosis by PG specific *wurst* knockdown revealed unusually strong Obst-A accumulation at the entire PG surface in stage 17 embryos (Fig. 6E;S3E). Resembling the *obst-A* knockdown phenotypes, Fas2 positive axon-like structures at the PG were not observed in PG specific UAS-*wurst* RNAi (Stümpges and Behr, 2011) knockdown embryos (Fig. 6E). The PG specific *wurst* knockdown caused lethality at the transition from first to second instar, growth arrest, and retained cuticles (Fig. 5B-D). *wurst* knockdown-like Obst-A accumulation at the ring gland surface and larval lethality were observed upon PG specific expression of a dynamin dominant negative mutation (Figs. 5D,6F,G) that is known to block clathrin-mediated endocytosis (Moline et al., 1999). In summary, our findings suggest that Wurst/Dynamin-mediated endocytosis is necessary for the internalization of Obst-A. These dynamics influence extracellular matrix properties which impact Fas2 positive axon-like structures at the late embryonic PG cells and subsequent molting events during larval transitions.

4. Discussion

We identified Obst-A as a specific extracellular component to the PG. Loss of *obst-A* and the PG-specific *obst-A* knockdown caused a range of phenotypes characteristic of ecdysone deficiency mutants. A PG specific requirement of Obst-A was further confirmed by the fact that CA (Aug21-Gal4) and CC (*akh*-Gal4 driven) specific *obst-A* knockdown did not result in ring gland defects, retained cuticles or

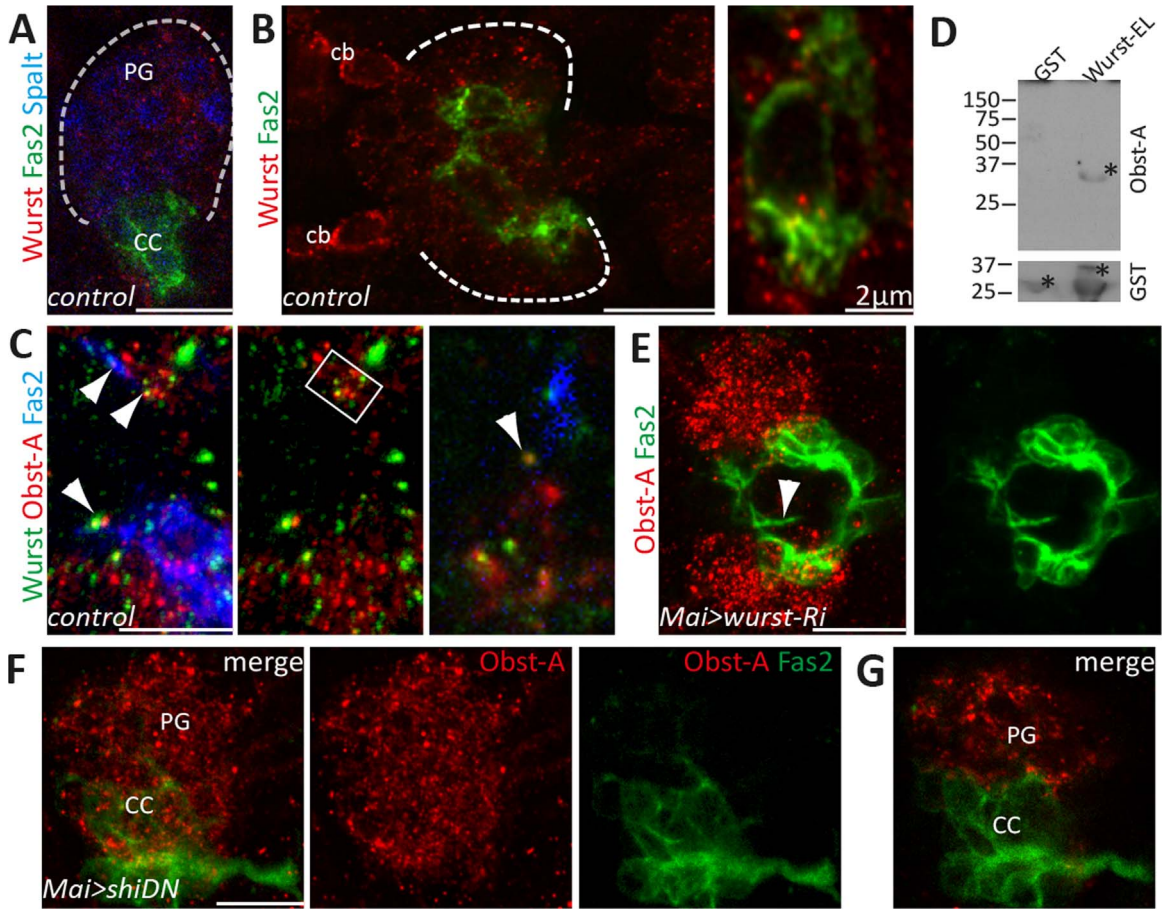

Fig. 6. PG specific Obst-A localization and axon formation depends on Wurst and Dynamin-mediated endocytosis. (A) Confocal image of stage 16 embryo shows Spalt staining in the PG cells, Fas2 positive CC cells and the overlapping expression with Wurst (red). (B) Confocal image of stage 17 embryo shows Wurst distribution in PG cells. The cerebral tracheal branches (cb) reaching to the PG (encircled by white dashes) express Wurst, too. Right hand image shows magnification of overlapping Wurst and Fas2 staining (Airyscan image). (C) In stage 17 *wt* embryos Wurst (green) staining overlaps with Obst-A (red) at the PG cells and Fas2 (blue) positive nerves (arrowheads). White frame in the middle image indicates the higher magnification presented in the right image. (D) Obst-A (~26.5 kDa) is pulled down from embryo extracts by the Wurst extracellular loop fused with GST (~30 kDa). The GST control is indicated below. (E) The PG specific Mai60-Gal4 driven *wurst* RNAi knockdown mutant stage 17 embryo showed unusual Obst-A accumulation at the PG surface (n = 5). Fas2 nerves that innervate the PG were not observed, but instead misrouted (arrowhead). Three-dimensional projections of confocal Z-stacks. (F,G) Mai60-Gal4 driven *dynamin* (UAS-shi^{DN}) dominant negative mutant stage 17 embryo showed Obst-A accumulation at the PG surface (n = 5). Fas2 axon-like structures at the PG surface were not observed in the endocytosis mutants. F, three-dimensional projection; G, confocal image. PG, prothoracic gland; CC, corpora cardiaca; cb, cerebral tracheal branch; Scale bars represent 10 µm if not otherwise indicated.

larval lethality. Mutant studies show the requirement of Obst-A at the PG cell surface for axon formation and the pulsatile up-regulation of genes involved in ecdysone machinery. Thus, our work demonstrates the importance of the PG specific extracellular matrix for ring gland morphology and physiology during late embryonic and early larval development.

4.1. Obst-A is required for regulation of steroidogenic genes

A recent study provided evidence that the circadian clock is a key driver of steroid hormone production. Steroidogenic genes, appeared selectively expressed at night and day in the third instar ring gland. It was shown that Halloween gene expression was dependent on Timeless, which couples the circadian machinery directly to steroid synthesis. Interestingly and comparable with Halloween genes, *obst-A* expression is under control of circadian rhythm depending on *timeless* and *period* in the PG cells (Di Cara and King-Jones, 2016, 2016).

Our *obst-A* mutant analysis show that most genes representative of ecdysteroidogenesis are prevented from regular pulse-like up-regulation prior to larval ecdysis. This includes even the primary ecdysone-inducible transcription factor E74A (Fig. 1A). Our findings are consistent with the observation of elevated *npc1a* but reduced *cyp18a* expression (Fig. S1B), suggesting that animals could try to raise ecdysone levels in *obst-A* mutants at the end of first instar development trying to restore the ability to molt. In the same context, application of the active 20E to first instar larvae had beneficial effect on survival when *obst-A* knocked down or completely absent, indicating that ecdysteroid production was prevented in the mutants. Although ecdysteroid application was beneficial, it did not rescue lethality to adulthood as was found for genes exclusively involved in ecdysone production (Niwa et al., 2010; Yoshiyama et al., 2006). Thus, on one hand partial rescue proves ecdysteroid deficiency caused by knockdown or loss of *obst-A* in the PG, on the other hand it shows that larvae suffer from severe defects in the tracheal and epidermal cuticles (Pesch et al., 2015; Petkau et al., 2012). Obst-A is not maternally contributed (Petkau et al., 2012) and ring gland Obst-A expression starts at late embryonic stage 16, indicating that Ecdysone signaling in earlier embryos cannot be affected by Obst-A (Kozlova and Thummel, 2003). By contrast, at molt from first to second instar *obst-A* mutants most likely become arrested when 20E levels rise. This would be consistent to our data showing reduced gene expression of ecdysteroidogenic factors in *obst-A* mutants.

4.2. Obst-A function at the PG cells is unique and chitin independent

At the cell surface Obst-A provides the capacity for binding chitin and associated proteins that modulate the chitin-matrix. Obst-A

controls the proper localization of chitin-deacetylases Serpentine (Serp) and Vermiform (Verm) and the chitin protector Knickkopf (Knk) (Behr and Hoch, 2005; Pesch et al., 2016, 2015; Petkau et al., 2012). The failure in forming a normal chitin-matrix in *obst-A* mutants disturbs tracheal and epidermal cuticle integrity and stiffness. Larvae lacking *obst-A* display wrinkled trachea and epidermis, as well as deformed body shape (Pesch et al., 2015; Petkau et al., 2012; Tiklova et al., 2013). However, lethality at larval transition, growth arrest, and retained cuticles found in *obst-A* mutant is typical for defects in the ecdysone pathway (Li and Bender, 2000). Consistent with this, a restricted Obst-A requirement in the cuticle would not explain why gene expression of *serp, verm* and *knk* failed to be up-regulated in *obst-A* mutant larvae in the onset of ecdysis (Pesch et al., 2015). In addition, none of these gene products were detected in the ring gland (Fig. S4). This altogether provides evidence for a PG specific but chitin-independent function of the Obst-A at the ring gland. Despite its tracheal expression Serp is secreted by the fat body, transported via hemolymph and taken up by tracheal cells (Dong et al., 2014). Thus, levels of free Serp molecules in the hemolymph could reflect the current status of chitin-matrix maturation and accompanied cuticle formation. We did not address whether Obst-A binds Serp also at the PG surface, but it would be a potential mechanisms to precisely sense the current status of developmental progress.

4.3. Obst-A defines a specific matrix at PG cells, which is required for axonal growth

The ECM provides a scaffold for cellular support and mediates many processes including signaling during morphogenesis and tissue homeostasis (Berrier and Yamada, 2007). Tissue stiffness enhances matrix-directed differentiation for example through nuclear Lamin-A to enhance tissue specific differentiation (Swift et al., 2013). Local tissue stiffness is critically involved in instructing neuronal growth, and softening of tissue leads to aberrant axon growth. Axons in softened brains dispersed from their normal trajectory showing reduced directionality, while axons grown on stiff substrates were longer than those on soft substrates (Koser et al., 2016). Our studies did not address the influences of Obst-A on PG matrix stiffness. But in analogy to its role in the cuticle (Petkau et al., 2012), where it modulates the chitin-matrix-properties, Obst-A may also influence extracellular matrix properties at PG cell surfaces in late embryos at a time when axons need to grow at the surfaces of the forming ring gland. We speculate that the lack of Obst-A may alter ECM composition, leading to local changes in matrix properties at the PG surfaces contributing to normal axon growth at the ring gland. This is consistent to our findings that inhibition of endocytosis led to phenotypes that were similar to PG specific *obst-A* knockdown (Fig. 5A-C), including larval lethality and lack of Fas2 axon-like structures at the PG (Fig. 4A). Thus, depending on axonal growth progress at the PG surface, local ECM properties underlie dynamic changes via endocytosis of factors, such as Obst-A, that may contribute to matrix stiffness. Since a direct affect was excluded by a general Obst-A overexpression in the PG cells, this model would explain the observed changes in the regular pattern of Fas2 axon-like structures in *obst-A* mutants, PG specific *obst-A* knockdown, and PG specific endocytic mutants.

5. Conclusion

Our study provide evidence that genetic regulation of ecdysone production in PG cells is under control of a specific ECM. We show that a chitin-binding protein, Obst-A, defines the surface of PG cells, thereby controlling larval survival, molting and growth. In addition to its role in the cuticle of epithelial organs, Obst-A supports function of PGs. By modulating the cell matrix Obst-A essentially contributes to axonal growth at the PG. Importantly, local matrix properties depend on Obst-A internalization by Wurst/Clathrin dependent endocytosis. Collectively, Obst-A provides a new link between the endocrine system, nervous system, and developmental growth control in insects and, due to evolutionary conservation of the *obstructor* gene family, potentially also in other arthropod species.

Acknowledgements

We are very thankful to the Bloomington and Vienna stock centers for providing fly stocks. We are very grateful to Michael B. O'Connor, Christen Mirth, Reinhard Bauer, Reinhard Schuh, Bernard Moussian, Lars Vollborn, Annemarie Hofmann, Achim Paululat and Stefan Luschnig for sharing flies and reagents. For AutoQuant deconvolution we appreciated assistance by Michael Mahlert (Bitplane). We are thankful to Amanda Haage, Thomas Magin, Rohan J. Khadilkar, and Christian Wolf for critical reading and corrections of the manuscript. We thank Kirst King-Jones for discussing data. We thank Laura CA Jussen and Miriam Richter for technical support. We are grateful to Michael Hoch, Reinhard Bauer and Thomas Magin and the members of the departments for stimulating atmosphere and research conditions. We thank Johannes Kacza and the Bioimaging Core Facility/Unit at the University of Leipzig for technical assistance. MB thanks the DFG for support (SFB645-C5).

Authors contributions

Y.Y.P & M.B designed the experiments and discussed data; Y.Y.P, R.H., T.A, and MB performed experiments and carried out data analysis; M.B. supervised the studies and wrote the manuscript.

Conflict of interests

The authors declare that no competing interest exist.

Appendix A. Supporting information

Supplementary data associated with this article can be found in the online version at doi:10.1016/j.ydbio.2018.10.007.

References

Araujo, S.J., Tear, G., 2003. Axon guidance mechanisms and molecules: lessons from invertebrates. Nat. Rev. Neurosci. 4 (11), 910–922. http://dx.doi.org/10.1038/nrn1243.

Bancalari, R.E., Gregory, L.C., McCabe, M.J., Dattani, M.T., 2012. Pituitary gland development: an update. Endocr. Dev. 23, 1–15. http://dx.doi.org/10.1159/000341733.

Barrio, R., Celis, J.F., de, Bolshakov, S., Kafatos, F.C., 1999. Identification of regulatory regions driving the expression of the Drosophila spalt complex at different developmental stages. Dev. Biol. 215 (1), 33–47. http://dx.doi.org/10.1006/dbio.1999.9434.

Behr, M., Hoch, M., 2005. Identification of the novel evolutionary conserved obstructor multigene family in invertebrates. FEBS Lett. 579 (30), 6827–6833. http://dx.doi.org/10.1016/j.febslet.2005.11.021.

Behr, M., Wingen, C., Wolf, C., Schuh, R., Hoch, M., 2007. Wurst is essential for airway clearance and respiratory-tube size control. Nat. Cell Biol. 9 (7), 847–853. http://dx.doi.org/10.1038/ncb1611.

Berrier, A.L., Yamada, K.M., 2007. Cell-matrix adhesion. J. Cell. Physiol. 213 (3), 565–573. http://dx.doi.org/10.1002/jcp.21237.

Danielsen, E.T., Moeller, M.E., Dorry, E., Komura-Kawa, T., Fujimoto, Y., Troelsen, J.T., Herder, R., O'Connor, M.B., Niwa, R., Rewitz, K.F., 2014. Transcriptional control of steroid biosynthesis genes in the Drosophila prothoracic gland by ventral veins lacking and knirps. PLoS Genet. 10 (6), e1004343. http://dx.doi.org/10.1371/journal.pgen.1004343.

Danielsen, E.T., Moeller, M.E., Yamanaka, N., Ou, Q., Laursen, J.M., Soenderholm, C., Zhuo, R., Phelps, B., Tang, K., Zeng, J., Kondo, S., Nielsen, C.H., Harvald, E.B., Faergeman, N.J., Haley, M.J., O'Connor, K.A., King-Jones, K., O'Connor, M.B., Rewitz, K.F., 2016. A Drosophila genome-wide screen identifies regulators of steroid hormone production and developmental timing. Dev. Cell 37 (6), 558–570. http://dx.doi.org/10.1016/j.devcel.2016.05.015.

Di Cara, F., King-Jones, K., 2013. How clocks and hormones act in concert to control the timing of insect development. Curr. Top. Dev. Biol. 105, 1–36. http://dx.doi.org/

10.1016/B978-0-12-396968-2.00001-4.
Di Cara, F., King-Jones, K., 2016. The circadian clock is a key driver of steroid hormone production in Drosophila. Curr. Biol.: CB 26 (18), 2469–2477. http://dx.doi.org/10.1016/j.cub.2016.07.004.
Dong, B., Miao, G., Hayashi, S., 2014. A fat body-derived apical extracellular matrix enzyme is transported to the tracheal lumen and is required for tube morphogenesis in Drosophila. Development 141 (21), 4104–4109. http://dx.doi.org/10.1242/dev.109975.
Gates, J., Lam, G., Ortiz, J.A., Losson, R., Thummel, C.S., 2004. rigor mortis encodes a novel nuclear receptor interacting protein required for ecdysone signaling during Drosophila larval development. Development 131 (1), 25–36. http://dx.doi.org/10.1242/dev.00920.
Gaziova, I., Bonnette, P.C., Henrich, V.C., Jindra, M., 2004. Cell-autonomous roles of the ecdysoneless gene in Drosophila development and oogenesis. Development 131 (11), 2715–2725. http://dx.doi.org/10.1242/dev.01143.
Hartenstein, V., 2006. The neuroendocrine system of invertebrates: a developmental and evolutionary perspective. J. Endocrinol. 190 (3), 555–570. http://dx.doi.org/10.1677/joe.1.06964.
Hsu, J.-Y., Sun, Z.-W., Li, X., Reuben, M., Tatchell, K., Bishop, D.K., Grushcow, J.M., Brame, C.J., Caldwell, J.A., Hunt, D.F., Lin, R., Smith, M.M., Allis, C.D., 2000. Mitotic phosphorylation of histone H3 is governed by Ipl1/aurora kinase and Glc7/PP1 phosphatase in budding yeast and nematodes. Cell 102 (3), 279–291. http://dx.doi.org/10.1016/S0092-8674(00)00034-9.
Huang, X., Suyama, K., Buchanan, J., Zhu, A.J., Scott, M.P., 2005. A Drosophila model of the Niemann-Pick type C lysosome storage disease: dnpc1a is required for molting and sterol homeostasis. Development 132 (22), 5115–5124. http://dx.doi.org/10.1242/dev.02079.
Jasrapuria, S., Arakane, Y., Osman, G., Kramer, K.J., Beeman, R.W., Muthukrishnan, S., 2010. Genes encoding proteins with peritrophin A-type chitin-binding domains in Tribolium castaneum are grouped into three distinct families based on phylogeny, expression and function. Insect Biochem. Mol. Biol. 40 (3), 214–227. http://dx.doi.org/10.1016/j.ibmb.2010.01.011.
Jindra, M., Palli, S.R., Riddiford, L.M., 2013. The juvenile hormone signaling pathway in insect development. Annu. Rev. Entomol. 58, 181–204. http://dx.doi.org/10.1146/annurev-ento-120811-153700.
Johnson, A.N., Mokalled, M.H., Haden, T.N., Olson, E.N., 2011. JAK/Stat signaling regulates heart precursor diversification in Drosophila. Development 138 (21), 4627–4638. http://dx.doi.org/10.1242/dev.071464.
Johnston, D.M., Sedkov, Y., Petruk, S., Riley, K.M., Fujioka, M., Jaynes, J.B., Mazo, A., 2011. Ecdysone- and NO-mediated gene regulation by competing EcR/Usp and E75A nuclear receptors during Drosophila development. Mol. Cell 44 (1), 51–61. http://dx.doi.org/10.1016/j.molcel.2011.07.033.
Kim, S.K., Rulifson, E.J., 2004. Conserved mechanisms of glucose sensing and regulation by Drosophila corpora cardiaca cells. Nature 431 (7006), 316–320. http://dx.doi.org/10.1038/nature02897.
Kingan, T.G., Gray, W., Zitnan, D., Adams, M.E., 1997. Regulation of ecdysis-triggering hormone release by eclosion hormone. J. Exp. Biol. 200 (Pt 24), 3245–3256.
King-Jones, K., Thummel, C.S., 2005. Nuclear receptors–a perspective from Drosophila. Nat. Rev. Genet. 6 (4), 311–323. http://dx.doi.org/10.1038/nrg1581.
Koser, D.E., Thompson, A.J., Foster, S.K., Dwivedy, A., Pillai, E.K., Sheridan, G.K., Svoboda, H., Viana, M., Costa, Ld.F., Guck, J., Holt, C.E., Franze, K., 2016. Mechanosensing is critical for axon growth in the developing brain. Nat. Neurosci. 19 (12), 1592–1598. http://dx.doi.org/10.1038/nn.4394.
Kozlova, T., Thummel, C.S., 2003. Essential roles for ecdysone signaling during Drosophila mid-embryonic development. Sciences 301 (5641), 1911–1914. http://dx.doi.org/10.1126/science.1087419.
Kruger, E., Mena, W., Lahr, E.C., Johnson, E.C., Ewer, J., 2015. Genetic analysis of Eclosion hormone action during Drosophila larval ecdysis. Development 142 (24), 4279–4287. http://dx.doi.org/10.1242/dev.126995.
Kruger, R.P., Aurandt, J., Guan, K.-L., 2005. Semaphorins command cells to move. Nat. Rev. Mol. Cell Biol. 6 (10), 789–800. http://dx.doi.org/10.1038/nrm1740.
Kuhnlein, R.P., Frommer, G., Friedrich, M., Gonzalez-Gaitan, M., Weber, A., Wagner-Bernholz, J.F., Gehring, W.J., Jackle, H., Schuh, R., 1994. spalt encodes an evolutionarily conserved zinc finger protein of novel structure which provides homeotic gene function in the head and tail region of the Drosophila embryo. EMBO J. 13 (1), 168–179.
Li, T., Bender, M., 2000. A conditional rescue system reveals essential functions for the ecdysone receptor (EcR) gene during molting and metamorphosis in Drosophila. Development 127 (13), 2897–2905.
Luschnig, S., Bätz, T., Armbruster, K., Krasnow, M.A., 2006. serpentine and vermiform encode matrix proteins with chitin binding and deacetylation domains that limit tracheal tube length in Drosophila. Curr. Biol. 16 (2), 186–194. http://dx.doi.org/10.1016/j.cub.2005.11.072.
McBrayer, Z., Ono, H., Shimell, M., Parvy, J.-P., Beckstead, R.B., Warren, J.T., Thummel, C.S., Dauphin-Villemant, C., Gilbert, L.I., O'Connor, M.B., 2007. Prothoracicotropic hormone regulates developmental timing and body size in Drosophila. Dev. Cell 13 (6), 857–871. http://dx.doi.org/10.1016/j.devcel.2007.11.003.
Melmed, S., 2003. Mechanisms for pituitary tumorigenesis: the plastic pituitary. J. Clin. Investig. 112 (11), 1603–1618. http://dx.doi.org/10.1172/JCI20401.
Mirth, C., Truman, J.W., Riddiford, L.M., 2005. The role of the prothoracic gland in determining critical weight for metamorphosis in Drosophila melanogaster. Curr. Biol.: CB 15 (20), 1796–1807. http://dx.doi.org/10.1016/j.cub.2005.09.017.
Moline, M.M., Southern, C., Bejsovec, A., 1999. Directionality of wingless protein transport influences epidermal patterning in the Drosophila embryo. Development 126 (19), 4375–4384.
Moussian, B., Tang, E., Tonning, A., Helms, S., Schwarz, H., Nusslein-Volhard, C., Uv, A.E., 2006. Drosophila Knickkopf and Retroactive are needed for epithelial tube growth and cuticle differentiation through their specific requirement for chitin filament organization. Development 133 (1), 163–171. http://dx.doi.org/10.1242/dev.02177.
Muglia, L.J., Bethin, K.E., Jacobson, L., Vogt, S.K., Majzoub, J.A., 2000. Pituitary-adrenal axis regulation in Crh-deficient mice. Endocr. Res. 26 (4), 1057–1066. http://dx.doi.org/10.3109/07435800009048638.
Niwa, R., Namiki, T., Ito, K., Shimada-Niwa, Y., Kiuchi, M., Kawaoka, S., Kayukawa, T., Banno, Y., Fujimoto, Y., Shigenobu, S., Kobayashi, S., Shimada, T., Katsuma, S., Shinoda, T., 2010. Non-molting glossy/shroud encodes a short-chain dehydrogenase/reductase that functions in the 'Black box' of the ecdysteroid biosynthesis pathway. Development 137 (12), 1991–1999. http://dx.doi.org/10.1242/dev.045641.
Niwa, R., Niwa, Y.S., 2014. Enzymes for ecdysteroid biosynthesis: their biological functions in insects and beyond. Biosci. Biotechnol. Biochem. 78 (8), 1283–1292. http://dx.doi.org/10.1080/09168451.2014.942250.
Nozumi, M., Nakatsu, F., Katoh, K., Igarashi, M., 2017. Coordinated movement of vesicles and actin bundles during nerve growth revealed by superresolution microscopy. Cell Rep. 18 (9), 2203–2216. http://dx.doi.org/10.1016/j.celrep.2017.02.008.
Ou, Q., Zeng, J., Yamanaka, N., Brakken-Thal, C., O'Connor, M.B., King-Jones, K., 2016. The insect prothoracic gland as a model for steroid hormone biosynthesis and regulation. Cell Rep. 16 (1), 247–262. http://dx.doi.org/10.1016/j.celrep.2016.05.053.
Park, Y., Filippov, V., Gill, S.S., Adams, M.E., 2002. Deletion of the ecdysis-triggering hormone gene leads to lethal ecdysis deficiency. Development 129 (2), 493–503.
Parvy, J.-P., Blais, C., Bernard, F., Warren, J.T., Petryk, A., Gilbert, L.I., O'Connor, M.B., Dauphin-Villemant, C., 2005. A role for betaFTZ-F1 in regulating ecdysteroid titers during post-embryonic development in Drosophila melanogaster. Dev. Biol. 282 (1), 84–94. http://dx.doi.org/10.1016/j.ydbio.2005.02.028.
Perrimon, N., Engstrom, L., Mahowald, A.P., 1985. Developmental genetics of the 2C-D region of the Drosophila X chromosome. Genetics 111 (1), 23–41.
Pesch, Y.-Y., Riedel, D., Behr, M., 2015. Obstructor A organizes matrix assembly at the apical cell surface to promote enzymatic cuticle maturation in Drosophila. J. Biol. Chem. 290 (16), 10071–10082. http://dx.doi.org/10.1074/jbc.M114.614933.
Pesch, Y.-Y., Riedel, D., Behr, M., 2017. Drosophila Chitinase 2 is expressed in chitin producing organs for cuticle formation. Arthropod Struct. Dev. 46 (1), 4–12. http://dx.doi.org/10.1016/j.asd.2016.11.002.
Pesch, Y.-Y., Riedel, D., Patil, K.R., Loch, G., Behr, M., 2016. Chitinases and Imaginal disc growth factors organize the extracellular matrix formation at barrier tissues in insects. Sci. Rep. 6, 18340. http://dx.doi.org/10.1038/srep18340.
Petkau, G., Wingen, C., Jussen, L.C.A., Radtke, T., Behr, M., 2012. Obstructor-A is required for epithelial extracellular matrix dynamics, exoskeleton function, and tubulogenesis. J. Biol. Chem. 287 (25), 21396–21405. http://dx.doi.org/10.1074/jbc.M112.359984.
Rewitz, K.F., Yamanaka, N., O'Connor, M.B., 2010. Steroid hormone inactivation is required during the juvenile-adult transition in Drosophila. Dev. Cell 19 (6), 895–902. http://dx.doi.org/10.1016/j.devcel.2010.10.021.
Rewitz, K.F., Yamanaka, N., O'Connor, M.B., 2013. Developmental checkpoints and feedback circuits time insect maturation. Curr. Top. Dev. Biol. 103, 1–33. http://dx.doi.org/10.1016/B978-0-12-385979-2.00001-0.
Riddiford, L.M., Truman, J.W., Mirth, C.K., Shen, Y.-C., 2010. A role for juvenile hormone in the prepupal development of Drosophila melanogaster. Development 137 (7), 1117–1126. http://dx.doi.org/10.1242/dev.037218.
Sanchez-Higueras, C., Sotillos, S., Castelli-Gair Hombria, J., 2014. Common origin of insect trachea and endocrine organs from a segmentally repeated precursor. Curr. Biol.: CB 24 (1), 76–81. http://dx.doi.org/10.1016/j.cub.2013.11.010.
Sánchez-Higueras, C., Hombría, J.C.-G., 2016. Precise long-range migration results from short-range stepwise migration during ring gland organogenesis. Dev. Biol. 414 (1), 45–57. http://dx.doi.org/10.1016/j.ydbio.2016.04.002.
Sapolsky, R.M., Romero, L.M., Munck, A.U., 2000. How do glucocorticoids influence stress responses? Integrating permissive, suppressive, stimulatory, and preparative actions. Endocr. Rev. 21 (1), 55–89. http://dx.doi.org/10.1210/edrv.21.1.0389.
Shimada-Niwa, Y., Niwa, R., 2014. Serotonergic neurons respond to nutrients and regulate the timing of steroid hormone biosynthesis in Drosophila. Nat. Commun. 5, 5778. http://dx.doi.org/10.1038/ncomms6778.
Siegmund, T., Korge, G., 2001. Innervation of the ring gland of Drosophila melanogaster. J. Comp. Neurol. 431 (4), 481–491. http://dx.doi.org/10.1002/1096-9861(20010319)431:4<481:AID-CNE1084>3.0.CO;2-7.
Stümpges, B., Behr, M., 2011. Time-specific regulation of airway clearance by the Drosophila J-domain transmembrane protein Wurst. FEBS Lett. 585 (20), 3316–3321. http://dx.doi.org/10.1016/j.febslet.2011.09.018.
Swift, J., Ivanovska, I.L., Buxboim, A., Harada, T., Dingal, P.C.D.P., Pinter, J., Pajerowski, J.D., Spinler, K.R., Shin, J.-W., Tewari, M., Rehfeldt, F., Speicher, D.W., Discher, D.E., 2013. Nuclear lamin-A scales with tissue stiffness and enhances matrix-directed differentiation. Science 341 (6149). http://dx.doi.org/10.1126/science.1240104.
Tajiri, R., Ogawa, N., Fujiwara, H., Kojima, T., 2017. Mechanical control of whole body shape by a single Cuticular protein obstructor-E in Drosophila melanogaster. PLoS Genet. 13 (1), e1006548. http://dx.doi.org/10.1371/journal.pgen.1006548.
Tiklova, K., Tsarouhas, V., Samakovlis, C., 2013. Control of airway tube diameter and integrity by secreted chitin-binding proteins in Drosophila. PLoS One 8 (6), e67415. http://dx.doi.org/10.1371/journal.pone.0067415.
Tojima, T., Itofusa, R., Kamiguchi, H., 2010. Asymmetric clathrin-mediated endocytosis

drives repulsive growth cone guidance. Neuron 66 (3), 370–377. http://dx.doi.org/10.1016/j.neuron.2010.04.007.

Uryu, O., Ou, Q., Komura-Kawa, T., Kamiyama, T., Iga, M., Syrzycka, M., Hirota, K., Kataoka, H., Honda, B.M., King-Jones, K., Niwa, R., 2018. Cooperative control of ecdysone biosynthesis in drosophila by transcription factors Seance, Ouija Board, and molting defective. Genetics 208 (2), 605–622. http://dx.doi.org/10.1534/genetics.117.300268.

Vaufrey, L., Balducci, C., Lafont, R., Prigent, C., Le Bras, S., 2018. Size matters! Aurora A controls Drosophila larval development. Dev. Biol. 440 (2), 88–98. http://dx.doi.org/10.1016/j.ydbio.2018.05.005.

Velasco, B., de, Erclik, T., Shy, D., Sclafani, J., Lipshitz, H., McInnes, R., Hartenstein, V., 2007. Specification and development of the pars intercerebralis and pars lateralis, neuroendocrine command centers in the Drosophila brain. Dev. Biol. 302 (1), 309–323. http://dx.doi.org/10.1016/j.ydbio.2006.09.035.

Velasco, B., de, Shen, J., Go, S., Hartenstein, V., 2004. Embryonic development of the Drosophila corpus cardiacum, a neuroendocrine gland with similarity to the vertebrate pituitary, is controlled by sine oculis and glass. Dev. Biol. 274 (2), 280–294. http://dx.doi.org/10.1016/j.ydbio.2004.07.015.

Walker, J.A., Gouzi, J.Y., Long, J.B., Huang, S., Maher, R.C., Xia, H., Khalil, K., Ray, A., van Vactor, D., Bernards, R., Bernards, A., 2013. Genetic and functional studies implicate synaptic overgrowth and ring gland cAMP/PKA signaling defects in the Drosophila melanogaster neurofibromatosis-1 growth deficiency. PLoS Genet. 9 (11), e1003958. http://dx.doi.org/10.1371/journal.pgen.1003958.

Wang, S., Meyer, H., Ochoa-Espinosa, A., Buchwald, U., Onel, S., Altenhein, B., Heinisch, J.J., Affolter, M., Paululat, A., 2012. GBF1 (Gartenzwerg)-dependent secretion is required for Drosophila tubulogenesis. J. Cell. Sci. 125 (Pt 2), 461–472. http://dx.doi.org/10.1242/jcs.092551.

Warren, J.T., Wismar, J., Subrahmanyam, B., Gilbert, L.I., 2001. Woc (without children) gene control of ecdysone biosynthesis in Drosophila melanogaster. Mol. Cell. Endocrinol. 181 (1–2), 1–14. http://dx.doi.org/10.1016/S0303-7207(01)00404-X.

Wingen, C., Stümpges, B., Hoch, M., Behr, M., 2009. Expression and localization of clathrin heavy chain in Drosophila melanogaster. Gene expression patterns. GEP 9 (7), 549–554. http://dx.doi.org/10.1016/j.gep.2009.06.007.

Yamada, M., Murata, T., Hirose, S., Lavorgna, G., Suzuki, E., Ueda, H., 2000. Temporally restricted expression of transcription factor betaFTZ-F1: significance for embryogenesis, molting and metamorphosis in Drosophila melanogaster. Development 127 (23), 5083–5092.

Yamanaka, N., Marqués, G., O'Connor, M.B., 2015. Vesicle-mediated steroid hormone secretion in Drosophila melanogaster. Cell 163 (4), 907–919. http://dx.doi.org/10.1016/j.cell.2015.10.022.

Yamanaka, N., Rewitz, K.F., O'Connor, M.B., 2013. Ecdysone control of developmental transitions: lessons from Drosophila research. Annu. Rev. Entomol. 58, 497–516. http://dx.doi.org/10.1146/annurev-ento-120811-153608.

Yeung, C.-M., Chan, C.-B., Leung, P.-S., Cheng, C.H.K., 2006. Cells of the anterior pituitary. Int. J. Biochem. Cell Biol. 38 (9), 1441–1449. http://dx.doi.org/10.1016/j.biocel.2006.02.012.

Yoshiyama, T., Namiki, T., Mita, K., Kataoka, H., Niwa, R., 2006. Neverland is an evolutionally conserved Rieske-domain protein that is essential for ecdysone synthesis and insect growth. Development 133 (13), 2565–2574. http://dx.doi.org/10.1242/dev.02428.

Yu, J., 2014. Endocrine disorders and the neurologic manifestations. Ann. Pediatr. Endocrinol. Metab. 19 (4), 184–190. http://dx.doi.org/10.6065/apem.2014.19.4.184.